Joint Centre for Mesoscale Meteorology, Reading, UK

Evolution of a mesoscale upper tropospheric vorticity maximum and comma cloud from a cloud-free two-dimensional potential vorticity anomaly

K. A. Browning

Internal Report No. 3

January 1993

Met Office Joint Centre for Mesoscale Meteorology Department of Meteorology
University of Reading PO Box 243 Reading RG6 6BB United Kingdom
Tel: +44 (0)118 931 8425 Fax: +44 (0)118 931 8791
www.metoffice.com

Evolution of a mesoscale upper tropospheric vorticity maximum and comma cloud from a cloud-free two-dimensional potential vorticity anomaly

K A Browning

Joint Centre for Mesoscale Meteorology*

University of Reading

Summary

A diagnostic case study is presented using output from the limited-area forecast version of the operational Meteorological Office Unified Model together with water vapour and cloud imagery from Meteosat. The case chosen for study was an archetypally simple example in which a long, narrow strip of air with high potential vorticity (PV) in the upper troposphere - strictly a tropopause depression - became unstable and rolled up into fairly long-lived mesoscale vortices. For much of the time the vortices were cloud-free and they were dynamically pure examples of very small upper air PV anomalies moving relative to the strata beneath. As such they provided a good test of theoretical deductions from the PV invertability principle and of the performance of the dynamical components of the forecast model.

footnote

*The Joint Centre for Mesoscale Meteorology is supported by the Meteorological Office and the Department of Meteorology, University of Reading.

The evolution of the mesoscale vortices as revealed in the satellite imagery was well handled by the Unified Model indicating that the small scales were reproduced well by the model dynamics even though they were not fully defined by the routine observations fed into the model. A detailed analysis of one of the mesoscale vortices throughout its 3-day lifetime showed that its maximum potential vorticity and absolute vorticity decreased with time as it travelled within the circulation of a large scale anticyclonic gyre. By the end of the second day, when cloud first formed, the vortex had become a weak upper tropospheric shear line, 500 km long, sandwiched between a pair of anticyclonic mesoscale vortices 900 km apart.

The Meteosat imagery revealed a characteristic two-component structure both in the water vapour channel and, when the cloud eventually formed, in the infra-red too. This structure, which resembled that seen on other occasions, is explained in terms of a particular combination of vertical motion and advection in the region of sharp humidity gradients alongside dry stratospheric air that had intruded into the upper troposphere.

1. Introduction

The main stratospheric polar vortex is surrounded by what McIntyre and Palmer (1984) called a surf zone where breaking planetary waves lead to large meridional excursions of air carrying with it its characteristic value of potential vorticity (PV). As part of this process and its extension to lower altitudes, stratospheric air with high PV travels equatorwards and descends into the upper troposphere. Sometimes, as in the case presented here, it leads to filaments of high PV within the upper troposphere which eventually break up into blobs of horizontally isolated PV maxima, as has also been seen to occur at larger scales within the stratosphere itself (Clough et al 1985) and has been modelled by Juckes and McIntyre (1987). The PV filaments can, in the presence of a large-scale deformation field, resist disruption for some time (Dritschel et al 1991).

But when they eventually do roll up into vortices, the resulting PV maxima can also persist for up to several days during which they are accompanied by characteristic dynamical structures as described by Hoskins et al (1985).

There are two important features associated with an upper tropospheric PV maximum. First, there is the rising motion that occurs just ahead of the PV maximum (when it is moving relative to the air below). Second, there is a region of reduced static stability directly beneath the PV anomaly (which does not depend on there being any relative motion). When a major incursion of high PV over-runs a region of moist air and strong baroclinicity it leads to rapid cyclogenesis, especially if the induced upward motion ahead of the incursion becomes moist ascent. Such events, which have attracted a lot of attention recently (e.g. Uccellini et al 1985, Whitaker et al 1988, Shutts 1990), involve strong non-linear interactions and diabatic effects, which generate important PV anomalies in the lower troposphere.

The system in the present study, by contrast, provided an opportunity to study simple dynamical effects in isolation. It was a relatively pure example of an upper level PV anomaly for which the lower level baroclinicity was weak and cloud absent until late in the system's evolution. Also the surface winds were light. Latent heat and surface friction therefore played little part in the dynamics of the system. The very simplicity of the system made it an ideal case for testing the performance of the dynamical components of a high-resolution forecast model.

The case in this paper involved the roll-up of part of a filament of high PV into three isolated PV maxima of mesoscale dimensions. Although only just big enough to show up on conventional synoptic charts, a careful analysis of one of these PV maxima using high-resolution NWP model

products showed that it nevertheless exhibited an overall dynamical structure like that associated with the mesoscale cold pool studied by Hill and Browning (1987) and the subsynoptic scale cold vortex/cold dome studied by Matsumoto et al (1982). It was also broadly similar to the much larger tropical disturbance analysed by Erickson (1971) and the large cut-off cyclones of the kind well known from the analyses of Palmén (1949) and Peltonen (1963). The initial PV filament in the present case was accompanied by an upper tropospheric shear line as discussed by Holopainen and Rontu (1981). In their case the separation of the regions of maximum winds on either side of the shear line was 1000 km and they regarded this as unusually small. In the present case the separation was 400 km and so this study is of a mesoscale system of a size not normally analysed in detail. The mesoscale PV anomaly produced characteristic signatures in satellite imagery - initially in the water vapour channel and later, when clouds formed, in the infra-red - and these will be explained in terms of the observed dynamical structure.

2. Data sources and data handling

The main sources of data used in this study are successive NWP model analyses from the operational limited area version of the Meteorological Office Unified Model (Cullen 1991), run at about 50 km grid spacing, and frequent digital images from Meteosat. Limited use is also made of data from the ECMWF model (T-106). The Unified Model analyses were employed at mainly 6-h intervals. Routine observational data are assimilated continuously into the Unified Model. The features of interest in this study were situated over the Atlantic to the west of France and the British Isles where the main source of observational input would have been in the form of aircraft reports.

Data from the Unified Model and from Meteosat were ingested into a VAX-based computer system at the Joint Centre for Mesoscale Meteorology and displayed using a PC-driven workstation (the 'DISP' display system developed by R Franks, C Court and T Hewson). For this purpose the grid spacing of the model data is degraded to 100 km and 100 mb. Resolution of the satellite data is about 5 km. The main limitation of the data set is that humidity is archived only at and below 300 mb; at higher levels it is set to zero. The workstation enables the model and satellite data to be registered and displayed together or separately, in colour and/or line contour format, with a capability for zoom and animation. Most standard model outputs are available on isobaric and, in the case of PV, on isentropic surfaces. Vertical sections with arbitrary orientation can also be displayed. The workstation proved invaluable in tracing the origins of the mesoscale dynamical system in this study which was first identified as an interesting case from inspection of the animated satellite imagery.

3. The broad context and origin of the mesoscale vortex

The mesoscale PV maximum that is the subject of this investigation occurred in a region dominated by a large anticyclone, far away from any frontal zones (Fig.1). Its most obvious manifestations to a forecaster would have been the weak trough in the thickness pattern over the British Isles (Fig.2) and the associated comma cloud that developed in the later stages of the vortex lifetime.

The mesoscale PV anomaly had its origin in a massive southward extension of high PV air in the upper troposphere over the Mediterranean a few days earlier. By 00Z on 15 January this area of high PV had elongated clockwise to produce a PV filament that trailed west over Spain and then northward over the Atlantic (Fig.3) (PV units are 10^{-6} $m^2 s^{-1}$ K kg^{-1}). The filament resembles, in an exaggerated form, what Hoskins et al (1985) referred to as a trailing trough (see their Fig 20(b)). It corresponds to

the LCI (lifecycle 1) paradigm of baroclinic wave behaviour of Thorncroft et al (1992). Anticyclonic behaviour dominates the evolution, which is characterized by backward-tilted, thinning troughs advected anticyclonically and equatorward, as in the commoner cases of planetary-scale mid-stratospheric Rossby-wave breaking. A cross-section through the filament 200 km northwest of the NW tip of Spain (Fig.4) reveals in miniature all the familiar features of an upper tropospheric shear line as analyzed by Holopainen and Rontu (1981), comprising a two-dimensional version of an upper-air cut-off cyclone structure: notice for example the region of dry subsided stratospheric air between the opposing upper jets overlying a region of diminished static stability in the middle troposphere. The evolution of this filament over the next three days is shown in Fig.5. By 00Z on the 16th a local maximum within the filament had become cut off southwest of Ireland. During the next two days this feature travelled as a closed contour with PV = 1 unit first towards Ireland and then across the British Isles before merging with the main region of high PV air to the north. It was not until about 00Z on the 17th that any cloud developed in association with the PV anomaly.

The PV filament decayed into only one blob easily resolvable on the 315 K isentropic surface (Fig.5), but slightly higher, on the 330 K surface (Fig.6), the filament can be seen decaying into three PV maxima, the middle one of which is the subject of this study. The wavelength of the instability that led to the break-up of the filament, estimated from the spacing of the maxima in Fig.6, was 900 km.

4. Three-dimensional structure of the evolving mesoscale vortex

The absolute vorticity associated with the mesoscale vortex was most intense at the 300 mb level. Fig.7(a) depicts the wind field and the pattern of absolute vorticity at that level for 4 times during the evolution of the vorticity maximum. Actual winds in the region surrounding

the vorticity maximum are shown on the left-hand side. The right-hand diagrams depict the winds relative to the motion of the vorticity maximum.

The sequence in Fig.7(a) shows the transition from an elongated shear line along the vorticity filament at 12Z/15th to an isolated mesoscale vorticity maximum at the later times. It shows how part of the elongated shear line rolled up into a compact vortex which itself evolved into a short cyclonic shear line. The latter can be seen at 00Z/17th acting as an interface between a pair of well-formed mesoscale anticyclonic vortices spaced 900 km apart along the direction of travel of the vorticity maximum (Fig.7(b)). The tendency for the atmosphere to become organized into anticyclonic circulations separated by thin cyclonic shear zones has been demonstrated at larger scales by Green et al (1966).

The 3-D dynamical structure of the evolving vorticity maximum is shown in the two sets of cross sections in Figs. 8a and 8b. The left hand columns show that the positive PV anomaly was most clearly identifiable between about 100 and 500 mb. (It is of course the isentropic gradient of PV that is dynamically fundamental, not other aspects of PV gradients; although isentropes are not plotted in Fig.8 their broad pattern would be similar to that shown in Fig.4). The patterns of absolute vorticity in Fig.8 show that although the absolute vorticity anomaly was greatest at 300 mb, it extended as a weak feature all the way down into the lower troposphere. The horizontal halfwidth (L) of the PV anomaly at the level of maximum absolute vorticity increased from 260 ± 20 km (in the direction transverse to the PV filament) at 00Z and 12Z on the 15th to about 450 ± 150 km at the later times. The maximum potential vorticity anomaly (P′) near the 300 mb level decreased by a quarter every 12 hours, from 6 units at 00Z/15th (Fig.4) to just under 2 units at 00Z/17th (Figs. 8a & b).

Joly and Thorpe (1990) have used linear instability analysis to investigate the development of secondary disturbances on a 2-D strip of high potential vorticity. Actually they studied a lower tropospheric strip of high PV generated by diabatic effects, but a similar analysis should apply to a filament of high PV in the upper troposphere. Like Dritschel et al (1991), they suggested that such a filament can be expected to remain stable so long as it is being stretched by a deformation field but that, once any such deformation weakens, it is susceptible to growth of linear normal modes along it. According to Thorpe (private communication), over a particular range of conditions, the wavelength (λ) of the resulting instability can be expected to be about ten times the half-width (L) of the PV anomaly divided by the magnitude of the PV anomaly (P′) expressed in PV units; this approximate relationship has been inferred from the analytical results shown in Joly and Thorpe (1990) which were derived on the basis of a PV anomaly in the range 0 to 2 units with a height scale of about a kilometre. The dependence on height scale is, in fact, not very strong. According to Waugh and Dritschel (1991), a large change in radius of deformation, roughly translating into a large change in strip height scale, makes little difference to the fastest growing wavelength. Taking the observed value of 260 km for L and a representative value of 2 units for P′ in the earliest stage of the roll-up of the filament (Fig.4), Thorpe's relationship gives a value of λ of 1300 km. A full linear stability calculation (G.C.Craig, private communication) using actual data from the present case gives a more accurate estimate of λ of 1100 km, and an e-folding time of 1.4 days. The predicted wavelength is close to the observed value of 900 km, and lends credence to the notion that the initial development was due to an instability of the PV strip.

The right-hand columns of Fig.8 (and also Fig.4 for the earlier time) show well-defined doublets in wind speed anomalies centred at 300 mb. The evolution of these wind anomalies and of the upper vorticity maximum is summarized in Fig.9. After an initial decrease during the first day, the absolute vorticity remained roughly constant. The peak wind component transverse to the direction of travel of the vortex increased slowly but erratically, at the expense of the parallel component which dropped from ± 30 ms^{-1} to almost zero, consistent with the vorticity maximum becoming a shear line rather than a symmetrical vortex.

5. Interpretation of Meteosat water vapour imagery in relation to the model-derived humidity pattern associated with the evolving mesoscale vortex

Fig.10 shows the model-derived humidity field at the 300 mb level, and Fig.11 shows the relative humidity within cross sections transverse (TT) and parallel (PP) to the motion of the vortex. The cross sections correspond exactly to those in Fig.8, showing that the vorticity maximum was located in the middle of these sections. At 00Z/16th the region of the vorticity maximum was characterised by very dry air with moist air just to the west; the weak ascent associated with it had produced only a marginal increase in humidity. By 12Z/16th the vorticity maximum had led to a more noticeable increase in humidity in its vicinity by a combination of local vortex-induced ascent and vortex-induced advection of the moist air from the west, leading to a hook-shaped distortion in the humidity field at 300 mb. By 00Z/17th the hook-shaped humidity feature had become accentuated (Fig.10); its vertical extent is seen to reach from above 300 mb down to 400 mb in Fig.11 where it is labelled A. The model-derived relative humidity in the vicinity of A increased from about 10% at 00Z/16th to 50% at 12Z/16th and then to 95% at 00Z/17th. Sustained ascent of 2 cm s^{-1} for 24 hours, corresponding to lifting through 1.7 km, is all that would have been needed to achieve this. This is consistent

with the model-derived vertical velocities; however, the instantaneous patterns of vertical velocity were somewhat noisy and so we have chosen to reproduce here only the patterns of relative humidity which because of their integrating effect do not appear to have suffered from this problem. Infra-red imagery from Meteosat discussed later showed that the first upper cloud appeared shortly after 00Z/17th.

The development of the hook-shaped mesoscale humidity pattern was seen in the imagery from the Meteosat 6.7 μm water vapour (WV) channel which is sensitive to the amount of water vapour in the upper troposphere. Fig.12 shows a sequence of space-view WV images for the period depicted in Fig.10. The feature of primary interest, seen towards the top left corner of each image, is sketched in Fig.13.

The satellite-observed location and timing of the developing hook-shaped humidity pattern are in remarkably close agreement with the model. There are, however, differences in the detailed structure which can be attributed to the lack of moisture in the archive of model data at 200 mb. Instead of the single major hook-shaped feature shown in the model at 00/17th (labelled A in Figs. 10 and 11), the WV imagery revealed two distinct humidity maxima (A and B in Fig.13). The occurrence of these two features is not a chance configuration for this one event: as discussed later (Section 7), the imagery reveals similar 2-component structures in the humidity distribution associated with other vorticity maxima on this occasion. Feature A, detected in the model at 300 and 400 mb, developed within initially dry air as a result of vortex-induced ascent plus some advection. Feature B, not evident in the model, appears to have been due mainly to vortex-induced advection at 200 mb of the pre-existing region of moist air that originally lay to the west of it. Evidence of the high level of Feature B is provided by the motion of this feature as seen by Meteosat. Detailed analysis of 2-hourly WV images showed that the leading edge of B travelled from 225^0 at 12 m s^{-1}, overtaking A at about 2 m s^{-1}.

The model indicated winds increasing by a similar amount between 300 and 200 mb.

6. Interpretation of the Meteosat infra-red imagery associated with the comma cloud

Upper cloud began to develop in association with humidity features A and B shortly after 00Z on 17 January. Fig.14 shows a sequence of reprojected Meteosat infra-red images depicting the development of the cloud. Fig.15, covering the same area as Fig.14, shows the relationship of the cloud (and the model-derived antecedent humidity anomaly) to the location of the PV maximum. It identifies the two cloud areas, A and B, that combined to form the comma cloud. Cloud areas A and B correspond to the humidity features A and B in the WV imagery.

The model-derived humidity feature, labelled A in Fig.14, relates well to the region where cloud A developed but, as noted above, the archived data from the model was not able to detect the higher level humidity feature. From 08Z onwards Cloud A had tops with brightness temperature (T_B) down to -52C whereas Cloud B had T_B as low as -65C. Assuming the T_B of the coldest, and presumably also the optically thickest, parts of the clouds corresponded to the true cloud top temperature, the tops of Clouds A and B would have been at 280 and 210 mb, respectively, in line with the heights inferred for the humidity features. There was a distinct height discontinuity between the two cloud features, consistent with the view that they originated from humidity features that were also distinct.

The two-component cloud structure in Fig.14 is reminiscent of that observed in association with so-called instant occlusions (Anderson et al 1969). The lambda-shaped cloud pattern in an instant occlusion occurs when a cloud band associated with a polar trough approaches and interacts with a pre-existing polar front cloud band. Although the present event was not an instant occlusion in these terms, there are close parallels. In both

cases there is a cut-off vorticity maximum aloft whose associated ascent generates a cloud band (A) and whose horizontal advection pattern distorts a pre-existing moist region giving rise to a second, orthogonal, cloud band (B). In the case of an instant occlusion the pre-existing moist region is a warm conveyor belt giving a cloud band along a polar front (Browning 1990). In the present case the vorticity maximum occurred near the boundary of a deep moist layer but there was hardly any baroclinicity and initially no cloud in the moist region. Nevertheless the vorticity maximum still went on to produce a two-component cloud pattern, with local vortex-induced ascent of dry air being the main factor in generating one of the cloud areas and vortex-induced local horizontal advection of a pre-existing moist region being the main factor in generating the other. The discontinuity between the two cloud features is associated with a residual region of dry air originating from the stratospheric air that subsided at the centre of the vorticity maximum. A similar feature is observed in instant occlusions (e.g. Browning and Hill 1985).

7. Identification of other mesoscale vortices from the imagery

The fact that dry air of stratospheric origin usually occurs in association with upper tropospheric vorticity maxima suggests that water vapour imagery should often be able to detect the early stages of vortex development. We have seen that, provided cloud does not obscure them, the resulting strong gradients in upper tropospheric moisture serve as good tracers of the developing instabilities. On this occasion three other such vorticity maxima were detected in this way, forming at different times from the same vorticity filament, although two of them were much smaller even than the one analysed above. Fig.16, depicting the imagery corresponding to these four vorticity maxima shows that each was characterised by the same two-component structure identified in Sections 5 & 6. They all formed on the edge of a thin dark strip in the water vapour imagery associated with the dry stratospheric air; the dark strip is best

portrayed early in the development of the main mesoscale vortex (see small arrow in Fig.12(a)).

8. Conclusions

A case study has been presented in which a breaking Rossby wave at tropopause level led to a filament of high potential vorticity in the upper troposphere that became unstable and broke into a set of mesoscale vorticity maxima with 900 km wavelength. The observed event is conceptually similar to breaking wave events that have been observed at larger scales, higher up in the stratosphere. One of the mesoscale vorticity maxima has been studied in detail; the others appeared to resemble it in many respects. Although they were cloud free for the first two days, a humidity discontinuity along the filament was distorted by each vortex instability. This, together with vortex-induced ascent, led to well defined roll-up signatures in the Meteosat water vapour (WV) imagery. The signature was especially clear cut because the region of moist air aloft was bounded by a very dry zone (WV dark zone) due to recently descended, and horizontally advected, stratospheric air.

Eventually the vortex-induced air motion led to the appearance of high level cirrus as seen in the infra-red imagery. There were two distinct components to the cloud pattern which appeared simultaneously and corresponded to two distinct features that had previously been observed developing in the WV imagery. One of these features, with a top just above 300 mb was due mainly to the lifting of dry air in the upper troposphere at the leading edge of the vortex; the other feature, with a top near 200 mb, was due to the advection of pre-existing moist air (plus a little ascent) around the right flank of the vortex. The two cloud components combined to form a comma cloud in a manner that is fairly commonly observed in the formation of so-called instant occlusions, suggesting that there may be some generality in the process described here, as expected from PV invertability.

The comma cloud developed over the Atlantic in a region where the only observations fed into the model would have been from aircraft reports. Nevertheless the time and location of appearance of the cloud was reproduced accurately by the Meteorological Office Unified Model which has thus been used with some confidence to diagnose the overall evolution in the dynamical structure of the mesoscale vortex. The quality of the model performance is attributed to the relative absence of complicating factors such as diabatic heating. The study suggests that, at least in these rather simple circumstances, an operational NWP model is capable of reproducing realistically the evolution of quite small atmospheric features, presumably because they are driven by larger scale motions that are sufficiently constrained by the model's assimilation of observational data. In other words these smaller scales are reproduced well by the model dynamics even though they are not fully defined by the observations fed into the model.

The mesoscale vortex developed as an instability on a long shear line across which there were opposing velocity maxima separated by 400 km that reached $\pm$ 30 m s^{-1} at the 300 mb level. The associated maximum absolute vorticity was large, almost 4 x 10^{-4} s^{-1}. It was predominantly an upper tropospheric phenomenon, the absolute vorticity diminishing to 1.5 x 10^{-4} s^{-1} by the 500 mb level. During the ensuing two days the region of large absolute vorticity remained confined to the upper troposphere and its maximum value decreased by a third. This decrease was associated with a decrease to almost zero in the component of the wind parallel to the motion of the vortex: thus the vortex after two days resembled a cyclonic shear line propagating almost at right angles to itself. This shear line was 500 km long and was sandwiched between two anticyclonic vortices separated by 900 km. The wind component parallel to, and on either side of, this mini-shear line had by the end of the second day increased from zero to about $\pm$ 14 m s^{-1}. It was at this stage that the comma cloud formed, being

detectable for a further day before merging with another system. The cloud remained confined to the upper troposphere and no precipitation whatsoever was detected by the weather radar network as it travelled across the British isles.

Acknowledgements

I am grateful to Dr P Ferris for generating model and satellite output from the DISP display system, to Prof A J Thorpe for suggestions concerning the instability of a PV strip, to Dr G C Craig for calculations relating to the fastest growing wavelength, and to Drs M E McIntyre and G J Shutts for their valuable comments on the draft manuscript. I wish to thank Mr G Sargent (Met Office) and Dr T Davies (ECMWF) for provision of data. The study relied heavily on the use of the versatile DISP system developed at the Joint Centre for Mesoscale Meteorology by R Franks, C Court and T Hewson under the direction of Dr S Clough.

References

Anderson, R.K. et al. 1969 'Application of meteorological satellite data in analysis and forecasting', ESSA Tech. Rep. NESC-51, US Dept of Commerce, Washington DC.

Browning, K.A. 1990 'Organization of clouds and precipitation in extratropical cyclones'. In Extratropical Cyclones: Erik Palmén Memorial Volume, Amer.Meteor.Soc, Boston, Mass, pp 129-153.

Browning, K.A., and Hill, F.F. 1985 'Mesoscale analysis of a polar trough interacting with a polar front'. Quart.J.R. Met.Soc., 111, 445-462.

Clough, S.A., Grahame, N.S. and O'Neill, A. 1985 'Potential vorticity in the stratosphere derived using data from satellites' Quart.J.R.Met.Soc., 111, 335-358.

Cullen,M.J.P. 1991 'The Unified Forecast/Climate Model'. Short Range Forecasting Division Scientific Paper No.1, Meteorological Office, Bracknell.

Dritschel,D.G., Haynes,P.H. Juckes,M.N. and Shepherd,T.G. 1991 'The stability of a two-dimensional vorticity filament under uniform strain'. J.Fluid Mech., 230, 647-665.

Erickson, C.D. 1971 'Diagnostic study of a tropical disturbance' Mon.Wea.Rev., 99, 67-78.

Green, J.S.A., Ludlam, F.H. and McIlveen, J.F.R. 1966 'Isentropic relative flow analysis and the parcel theory', Quart.J.R.Met.Soc, 92, 210-219

Hill, F F and Browning, K.A. 1987 'Case study of a persistent mesoscale cold pool'. Meteor.Mag., 116, 297-309.

Holopainen, E.O. and Rontu, L. 1981 'On shear lines in the upper troposphere over Europe', Tellus, 33, 351-359

Hoskins, B.J., McIntyre, M.E. and Robertson, A.W. 1985 'On the use and significance of isentropic potential vorticity maps', Quart.J.R.Met.Soc, 111, 877-946 and corrigendum 113, 402-404.

Joly, A and Thorpe, A.J. 1990 'Frontal instability generated by tropospheric potential vorticity anomalies' Quart.J.R.Met.Soc., 116, 525-560

Juckes, M.N. and McIntyre, M.E. 1987 'A high-resolution one-layer model of breaking planetary waves in the stratosphere', Nature, 328, 590-596.

Matsumoto, S., Ninomiya, K., Hasegawa, R. and Miki, Y. 1982 'The structure and the role of a subsynoptic-scale cold vortex on the heavy precipitation' J.Met.Soc.Japan, 60 339-353.

McIntyre, M.E. and Palmer, T.N. 1984 'The 'surf zone' in the stratosphere', J.Atm.Terr.Phys., 46, 825-849

Palmén, E. 1949 'Origin and structure of high-level cyclones south of the maximum westerlies', Tellus, 1, 22-31.

Peltonen, T. 1963 'A case study of an intense upper cyclone over eastern and northern Europe in November 1959'. Geophysica (Helsinki), 8, 225-251.

Shutts, G.J. 1990 'Dynamical aspects of the October storm, 1987: A study of a successful fine-mesh simulation'. Quart.J.R.Met.Soc, 116 1315-1347.

Thorncroft, C.D., Hoskins, B.J. and McIntyre, M.E. 1992 'Two paradigms of baroclinic-wave life cycle behaviour', Submitted for publication.

Uccellini, L.W., Brill, K.F. and Wash, C.H. 1985 'The President's Day cyclone of 18-19 February 1979: Influence of upstream trough amplification and associated tropopause folding on rapid cyclogenesis' Mon.Wea.Rev., 113, 962-988.

Waugh, D.W. and Dritschel, D.G. 1991 'The stability of filamentary vorticity in two-dimensional geophysical vortex-dynamics models', J.Fluid Mech., 231, 575-598

Whitaker, J.S., Uccellini, L.W. and Brill, K.F. 1988 'A model-based diagnostic study of the rapid development phase of the President's Day cyclone. Mon.Wea.Rev., 116, 2337-2365.

Figure Legends

Fig.1. Surface analysis for 00Z, 17 January 1992, from the European Meteorological Bulletin.

Fig.2. 1000-500 mb thickness and thermal wind analysis for 00Z, 17 January, 1992 from the European Meteorological Bulletin. The outline of the comma cloud associated with the upper PV maximum is also shown.

Fig.3. Potential vorticity exceeding 1 PV unit on the 315 K isentropic surface at 00Z, 15 January 1992. Air with PV in excess of 1 to 2 units is within the stratosphere or of recent stratospheric origin. Analysis from ECMWF (Courtesy T Davies).

Fig.4. Vertical section across the PV filament at 00Z 15 January 1992, at a location 200 km northwest of the NW tip of Spain, corresponding to where the mesoscale vortex developed 12 hours later. Potential temperature is shown by solid lines in degrees K. The wind component parallel to the filament is shown by dashed lines in m s^{-1} relative to the 7 m s^{-1} velocity of the mesoscale vortex. The tropopause (PV = 2 units) and the PV maximum (7 units) are shown by thick lines. The region of very dry air (RH < 10%) is shown shaded. This and subsequent analyses are from the Meteorological Office Unified Model.

Fig.5. Potential vorticity exceeding 1 PV unit on the 315 K isentropic surface at 6-hr intervals on 15, 16 and 17 January, 1992. Isopleths are at invervals of 1 PV unit. The PV maximum that is the focus of the case study is identified by a cross; its track from 12Z/15th onwards is shown in the bottom right-hand panel.

Fig.6. Evolution of the filament into discrete vortices on the 330 K isentropic surface at 6-hr intervals between 00Z, 15 January and 00Z, 17 January 1992. Isopleths are at intervals of 1 PV unit above

4 PV units. The 00Z/17th contours are plotted in their true position in relation to the coastlines; contours for other times are displaced to the left by a distance shown as 'd' for each 6-h interval. The PV maximum that is the focus of this study is marked by crosses.

Fig.7(a) Wind field at 300 mb in areas centred on the upper tropospheric vorticity maximum superimposed on the field of absolute vorticity (stippled $< 5 \times 10^{-5}$ s^{-1}, lightly stippled 5 to 15 x 10^{-5}, s^{-1}, white > 15 x 10^{-5} s^{-1}), at 12Z/15th. 00Z/16th, 12Z/16th and 00Z/17 January 1992. Left-hand diagrams: actual winds plus the location of the vertical sections TT and PP shown in Figs. 8a and 8b, respectively. Right-hand diagrams: winds relative to the motion of the vorticity maximum. Grid spacing is 100 km.

Fig.7(b) Schematic portrayal of the 300 mb flow relative to the motion of the vorticity maximum (X) at 00Z, 17 January 1992. The dashed line shows the 500 km long cyclonic shear line sandwiched between two anti-cyclonic vortices. The y-axis is drawn to correspond to the orientation of the flow within which the vorticity maximum is embedded.

Fig.8a. Vertical structure of the upper vorticity maximum within sections TT through its centre transverse to its direction of travel at 12Z/15th, 00Z/16th, 12Z/16th and 00Z/17 January 1992. The left hand diagrams show potential vorticity (contours at intervals of 1 PV; shaded for PV > 1 unit) and absolute vorticity (dashed contours at 5 x 10^{-5} s^{-1} intervals above 10 x 10^{-5} s^{-1}). The right-hand diagrams show the component of the wind parallel to the direction of travel of the vorticity maximum (contours at intervals of 2 m s^{-1}; air in shaded regions overtaking the upper vorticity maximum into the plane of the diagram).

Fig.8(b) Similar to (a) but for sections PP through the centre of the vorticity maximum oriented parallel to its direction of travel (front on right side). The right- hand diagrams show the component of the wind perpendicular to the direction of travel of the vorticity maximum (contours at intervals of 2 m s^{-1}; shaded for wind components toward left side of track).

Fig.9. Time history of the principal characteristics of the upper vorticity maximum, showing the peak values of the absolute vorticity (0) and of the wind components parallel (X) and perpendicular (+) to the direction of travel of the vortex, all at the 300 mb level.

Fig.10. Evolution of the humidity field associated with the upper vorticity maximum at 300 mb derived from the model at 6-h intervals between 00Z, 16 January and 00Z, 17 January 1992. Contours are at 50 and 70% relative humidity (solid) and 10% (dashed at 00Z/16th): areas moister than 50% are shaded. The contours at 00Z/17th are plotted in their true position in relation to the coastlines; contours at other times are displaced to the left by the distance shown as '1' for each 6-h interval. The dashed lines, PP and TT, show the orientation of the vertical sections in Fig.11.
The maximum of absolute vorticity at each time was located at the intersection of PP and TT.

Fig.11. Humidity structure of the upper vorticity maximum within cross-sections TT and PP through its centre transverse and parallel to its direction of travel, at 00Z/16th, 12Z/16th and 00Z/17 January 1992. Contours are for 10, 30, 50 and 70% relative humidity (shaded in excess of 50%). Humidity feature A is also identified in Fig.10 and later in Fig.15.

Fig.12. Sequence of space view Meteosat water vapour images at (a) 1755Z/15th, (b) 2355Z/15th (c) 0555Z/16th, (d) 1155Z/16th, (e) 1755Z/16th and (f) 0155Z/17 January 1992. Courtesy ESA and EUMETSAT. The brightness of the imagery is an indication of the humidity of the upper troposphere; bright areas are moist and the whitest areas contain upper cloud (although there is hardly any upper cloud in the region discussed in Section 5 except in the last frame - Fig.12f). The central half of each image is filled with relatively dry air bounded on the south and west by moist air, the curved interface between the dry and moist air corresponding to the remains of the major PV filament shown in Fig.3. The top left-hand portion of each image contains the mesoscale distortions in the water vapour boundary that began close to the head of the small arrow in (a) and culminated, after the time of (f), in the development of the comma cloud.

Fig.13. Outlines of parts of the WV images in Fig.12 drawing attention to the evolution of humidity features A and B discussed in the text. Stippled shading corresponds to high water vapour content in the upper troposphere. Hatched shading corresponds to high cloud. The pattern for 0155Z/17th is plotted in its true position in relation to the background map: patterns at other times are displaced successively to the left by the distance shown as 's'.

Fig.14. (a-f) Sequence of reprojected Meteosat infra-red images at 00Z, 03Z, 06Z, 08Z, 11Z and 13Z on 17 January 1992 showing the development of the comma cloud. White, pale, medium and dark grey areas, respectively, have brightness temperatures (T_B) colder than -55, -50, -20 and -10C; black areas have T_B warmer than -10C. All images have the same projection; to avoid cluttering them, the coastline and lat/long lines are shown only once. The comma cloud is a combination of two cloud areas identified as A and B in Fig.15.

Fig.15. Sketches of Meteosat cloud features A and B at two times (copied from Fig.14) and of the region of nearly saturated air corresponding to humidity feature A just prior to cloud formation (obtained from the model), shown in relation to successive positions of the 315 K PV maximum over the period 00 to 12Z on 17 January 1992.

Fig.16. Parts of the water vapour images from Meteosat, with sketches, for a (a) 1155Z/15th, (b) 0025Z/17th and (c) 0755Z/17 January 1992, showing four different upper vorticity maxima that formed from the same filament.

Fig. 1.

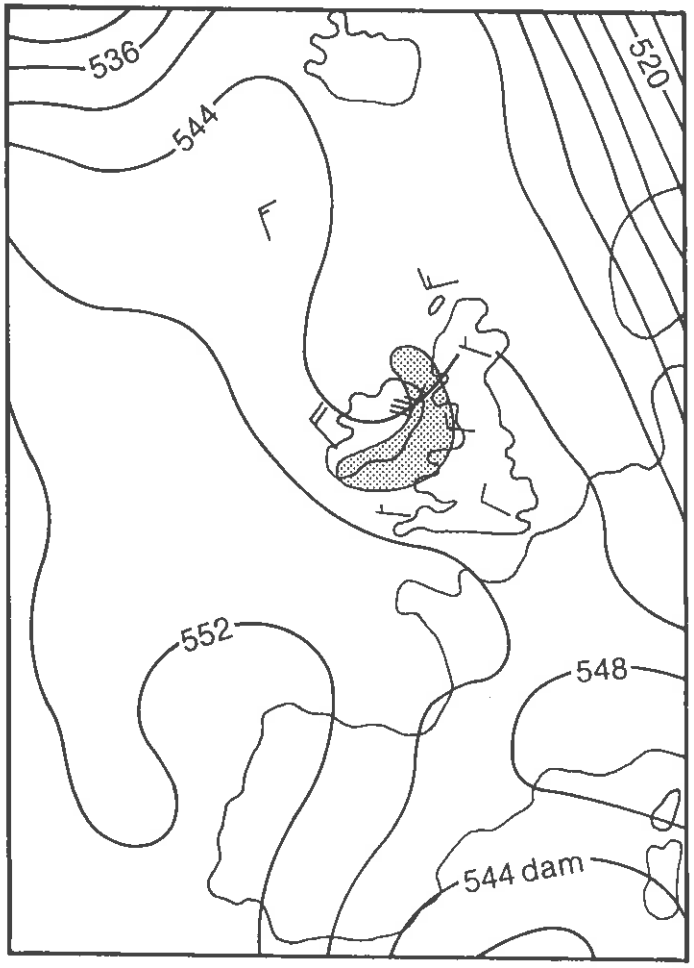

Fig. 2

00 UTC 15 Jan 1992

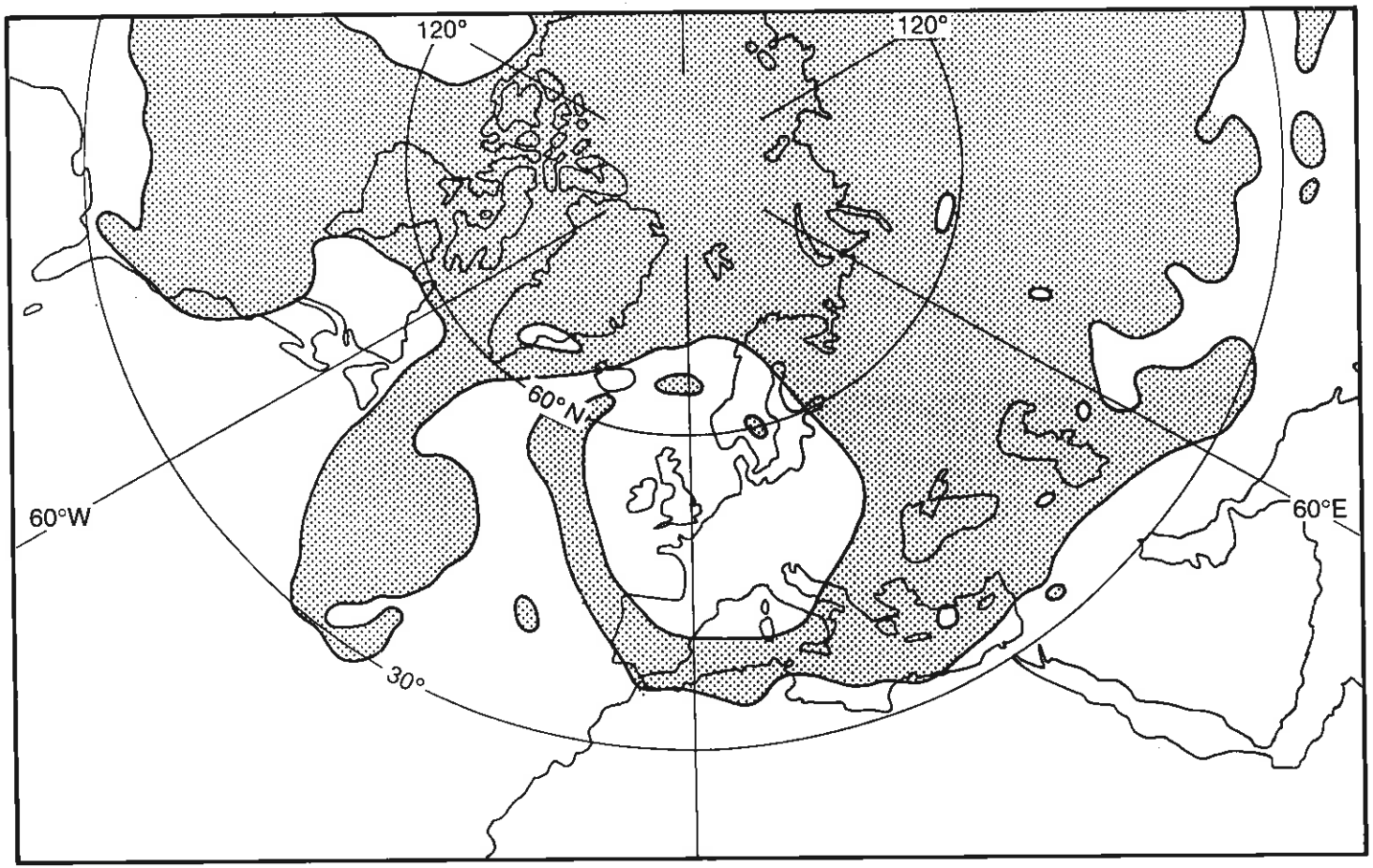

Fig 3

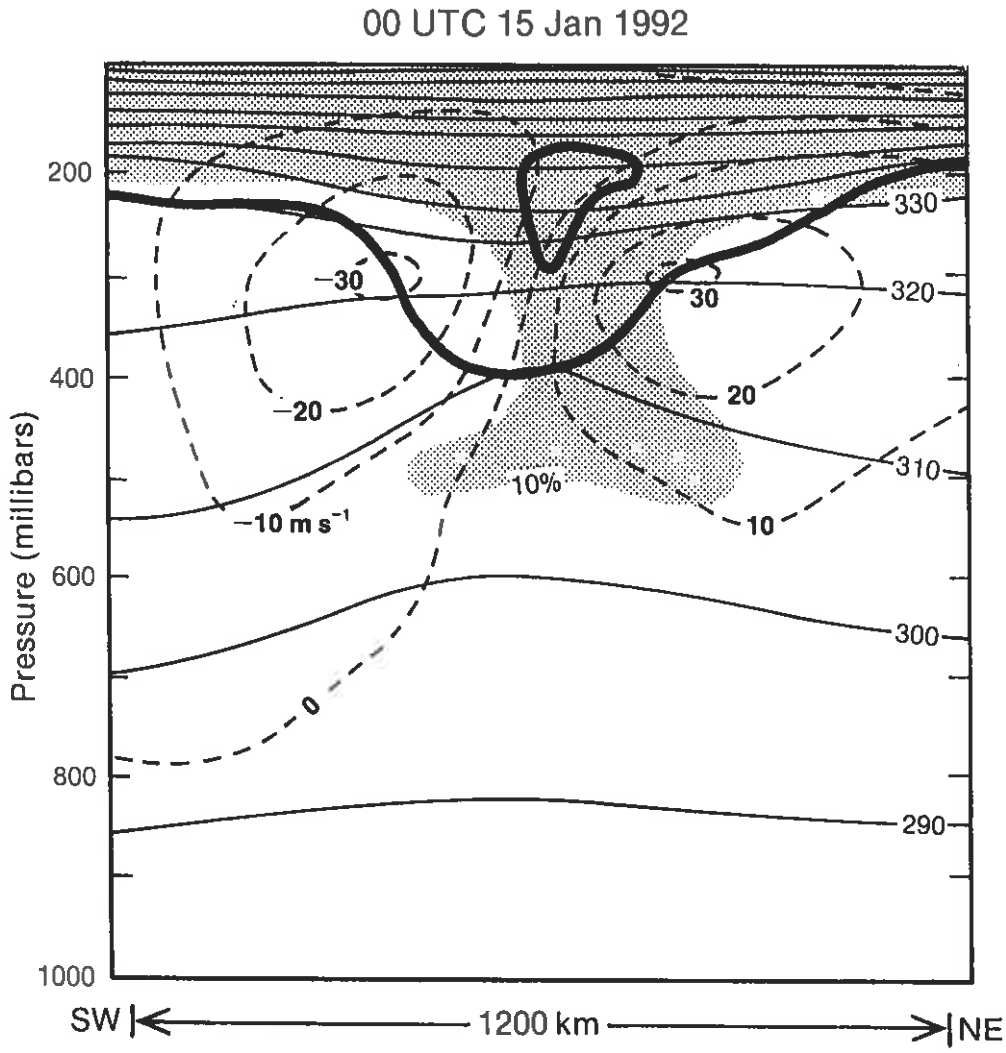
00 UTC 15 Jan 1992
Pressure (millibars)
200
400
600
800
1000
330
320
310
300
290
30
30
20
20
10
0
10%
10 m s⁻¹
SW
1200 km
NE

Fig 4

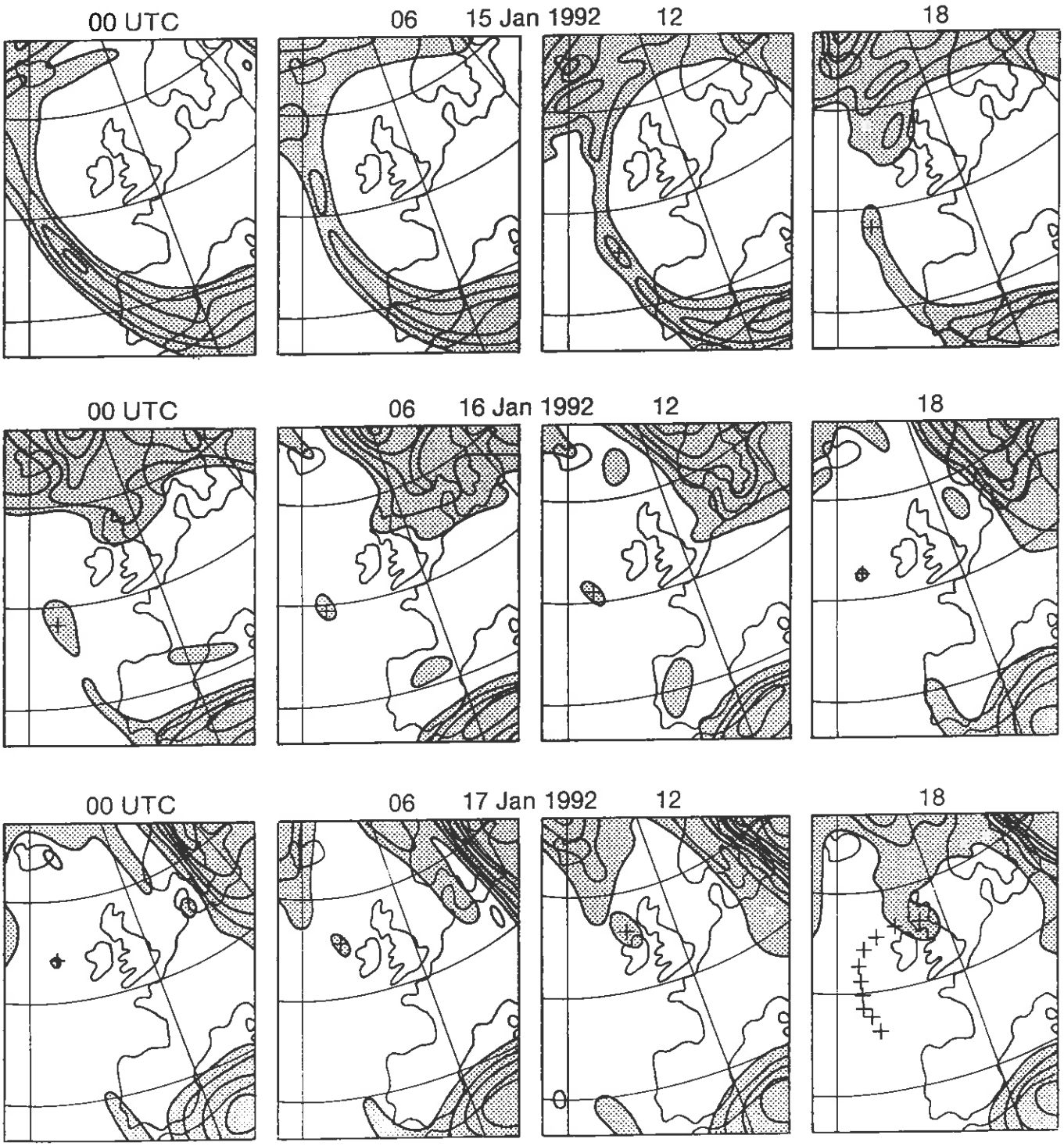
00 UTC
06
15 Jan 1992
12
18
00 UTC
06
16 Jan 1992
12
18
00 UTC
06
17 Jan 1992
12
18

Fig 5

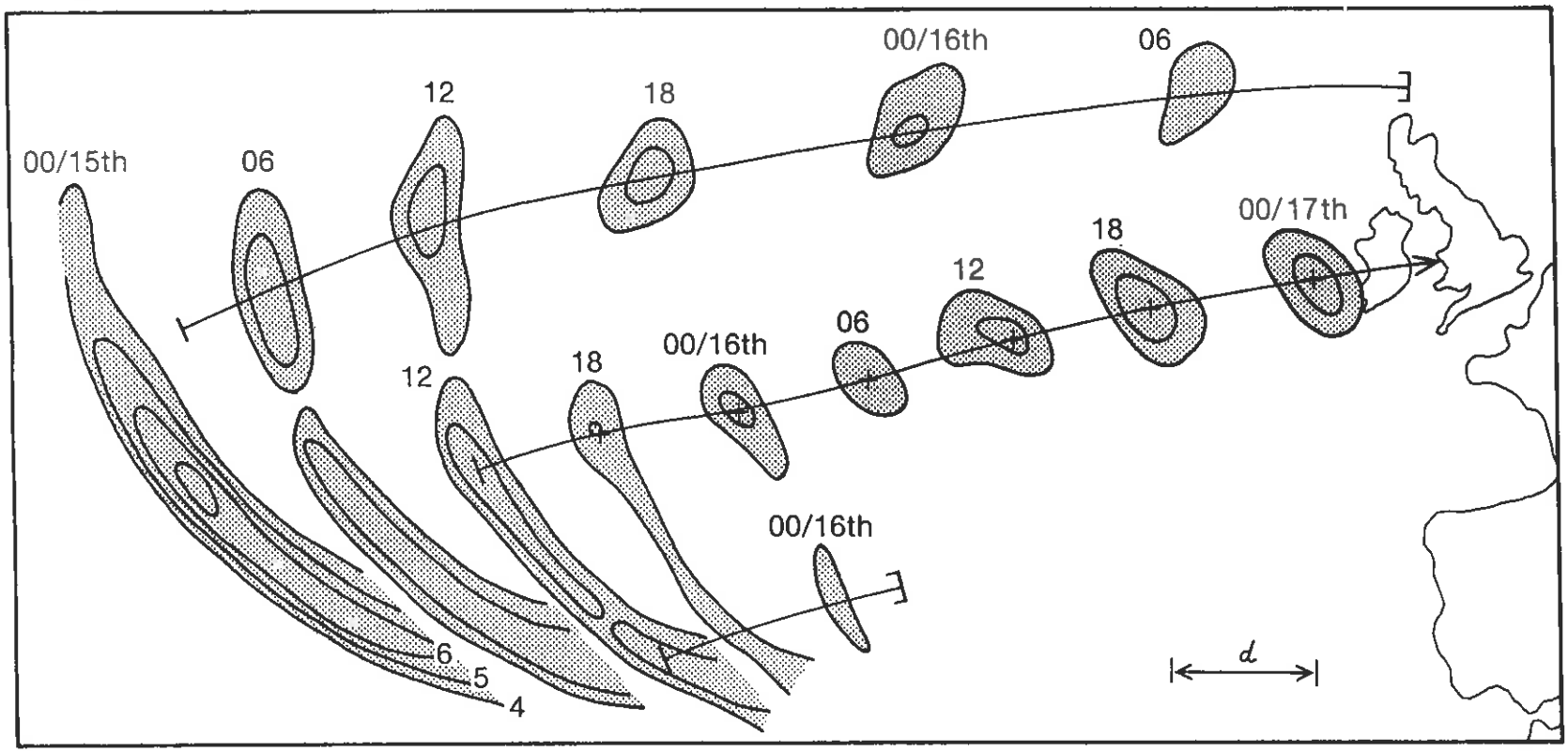
330 K PV
00/15th
06
12
18
00/16th
06
00/17th
18
12
06
00/16th
18
12
00/16th
6
5
4
d

Fig 6

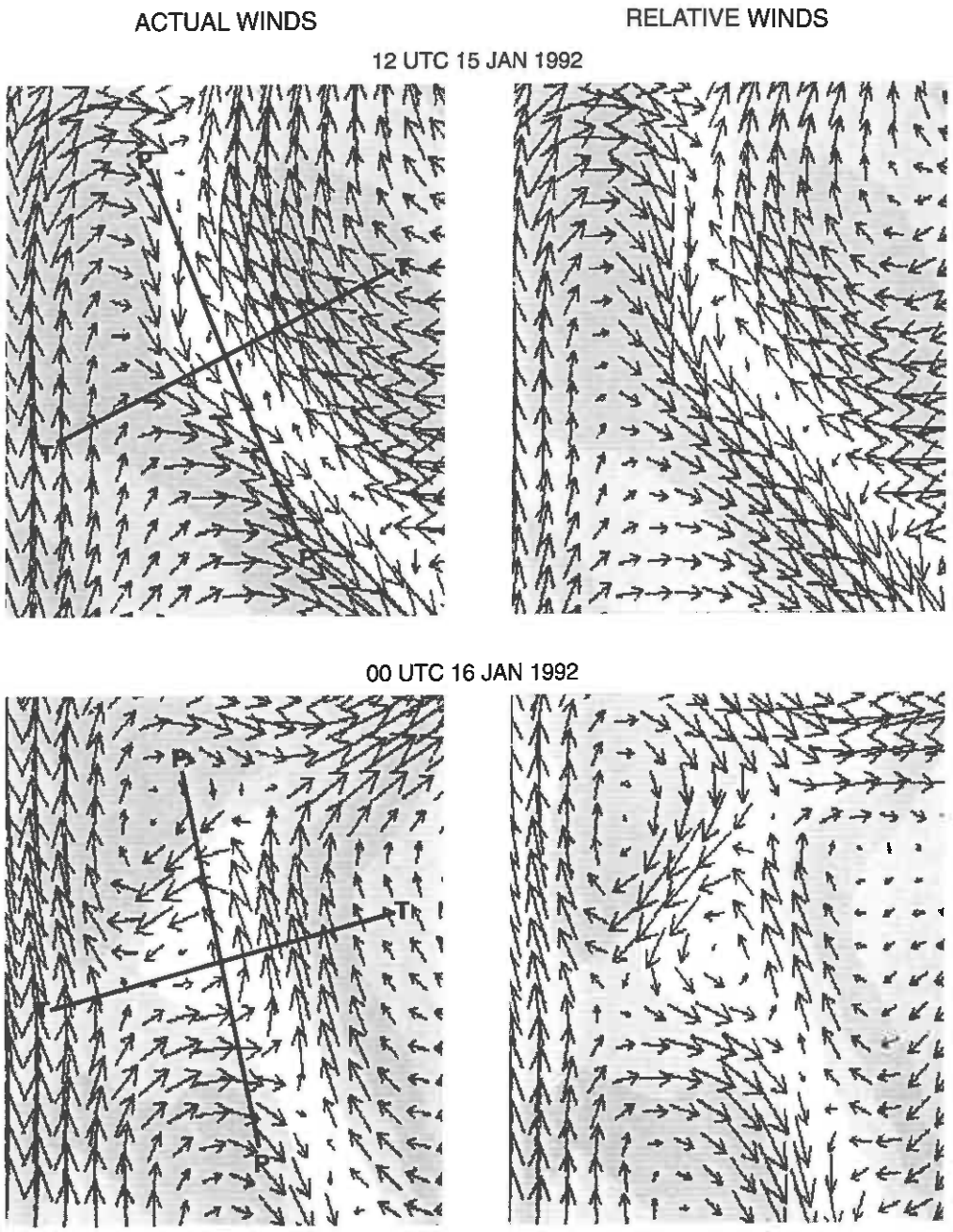
ACTUAL WINDS
RELATIVE WINDS
12 UTC 15 JAN 1992
00 UTC 16 JAN 1992

Figure 7(a) (i)

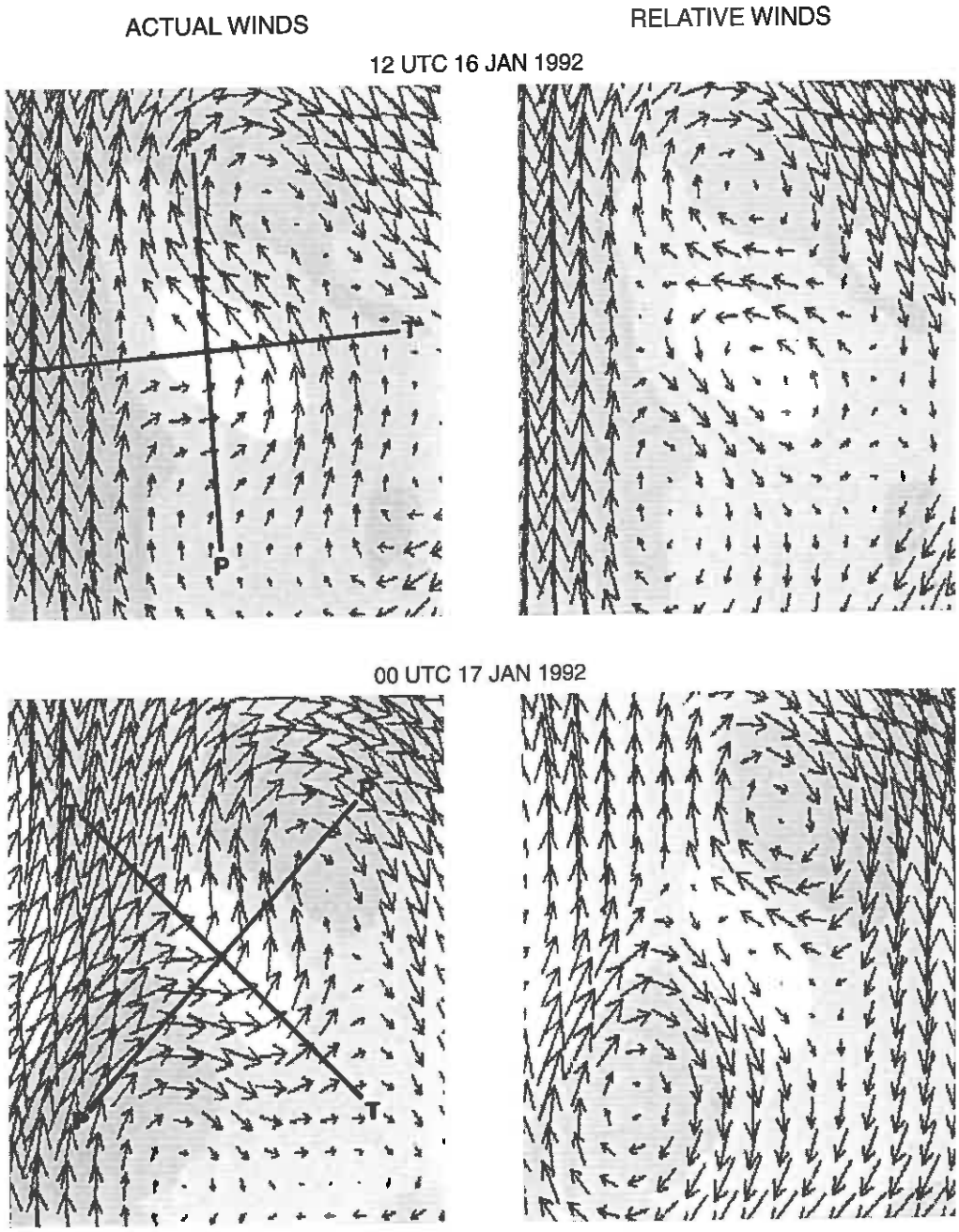
ACTUAL WINDS
RELATIVE WINDS
12 UTC 16 JAN 1992
P
T
00 UTC 17 JAN 1992
T

Figure 7(a) (ii)

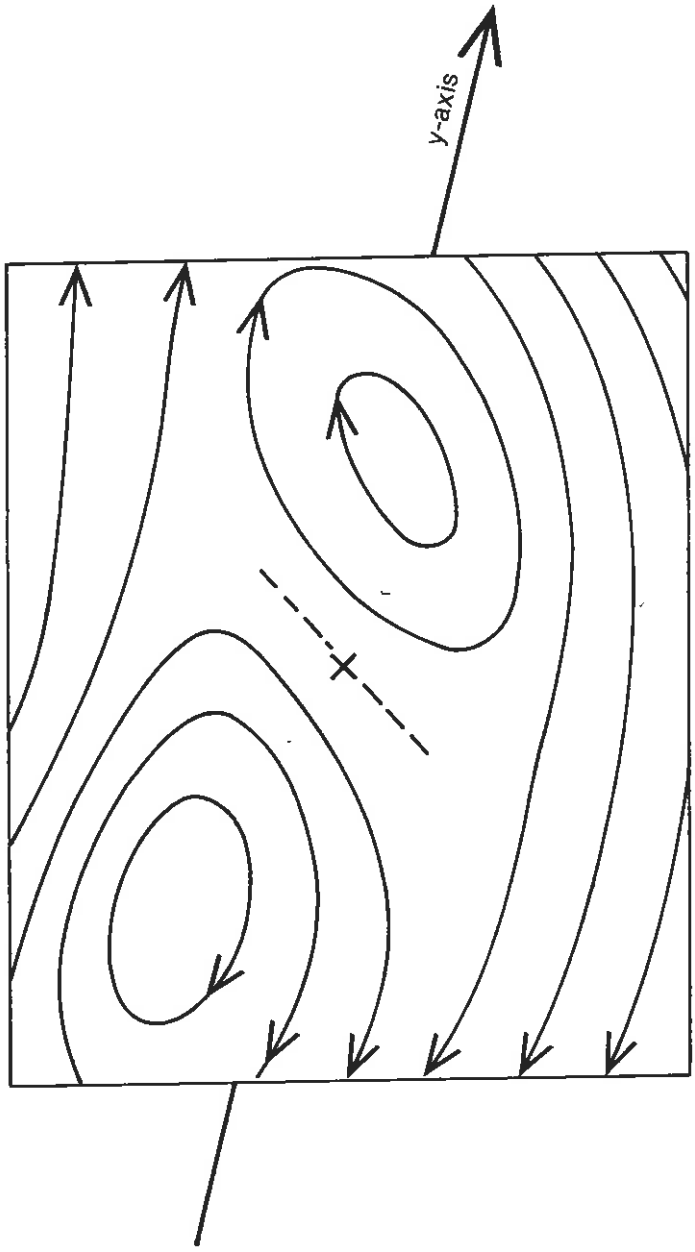

Fig. 7(b)

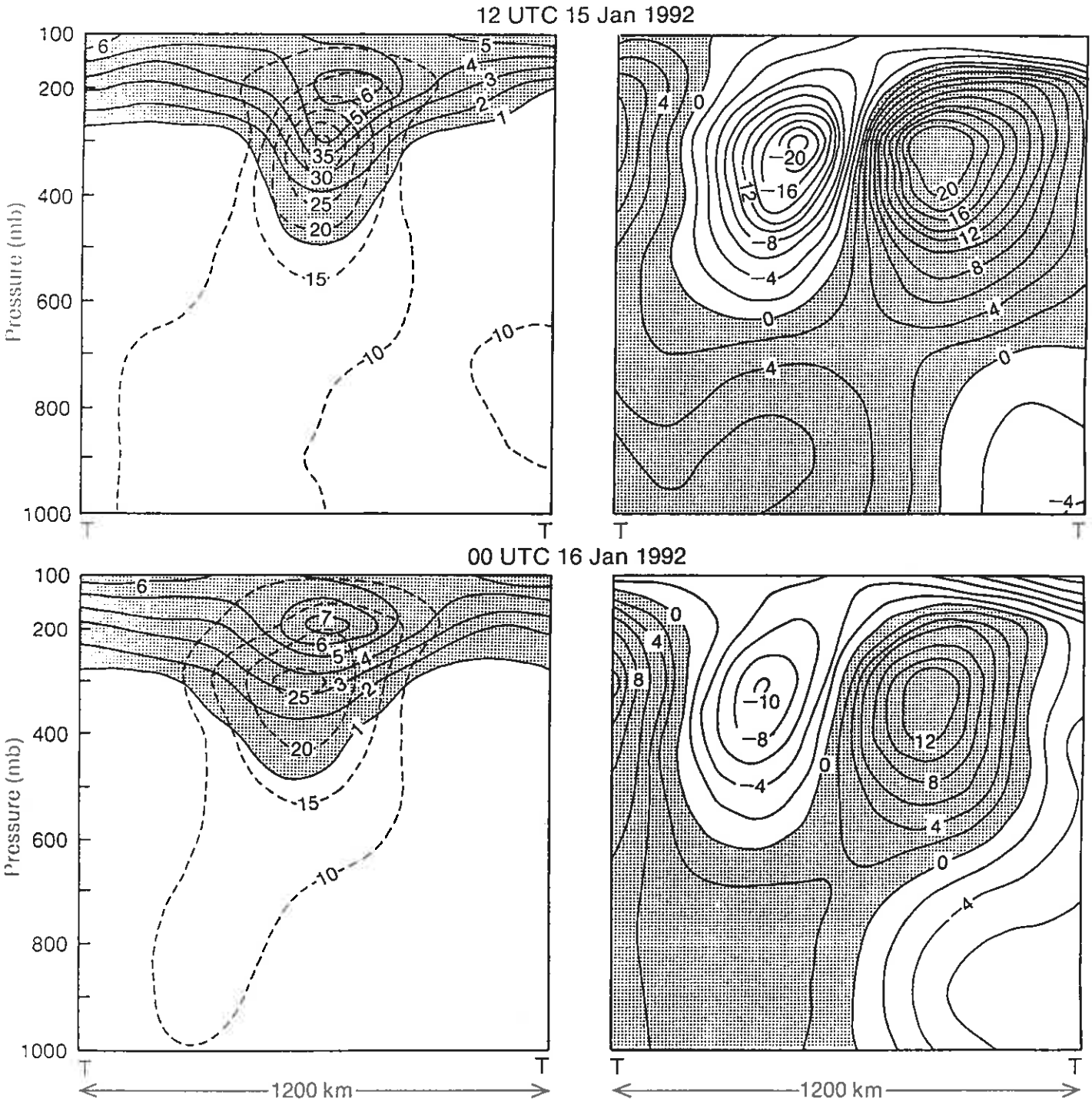

Fig 8(a) (first part)

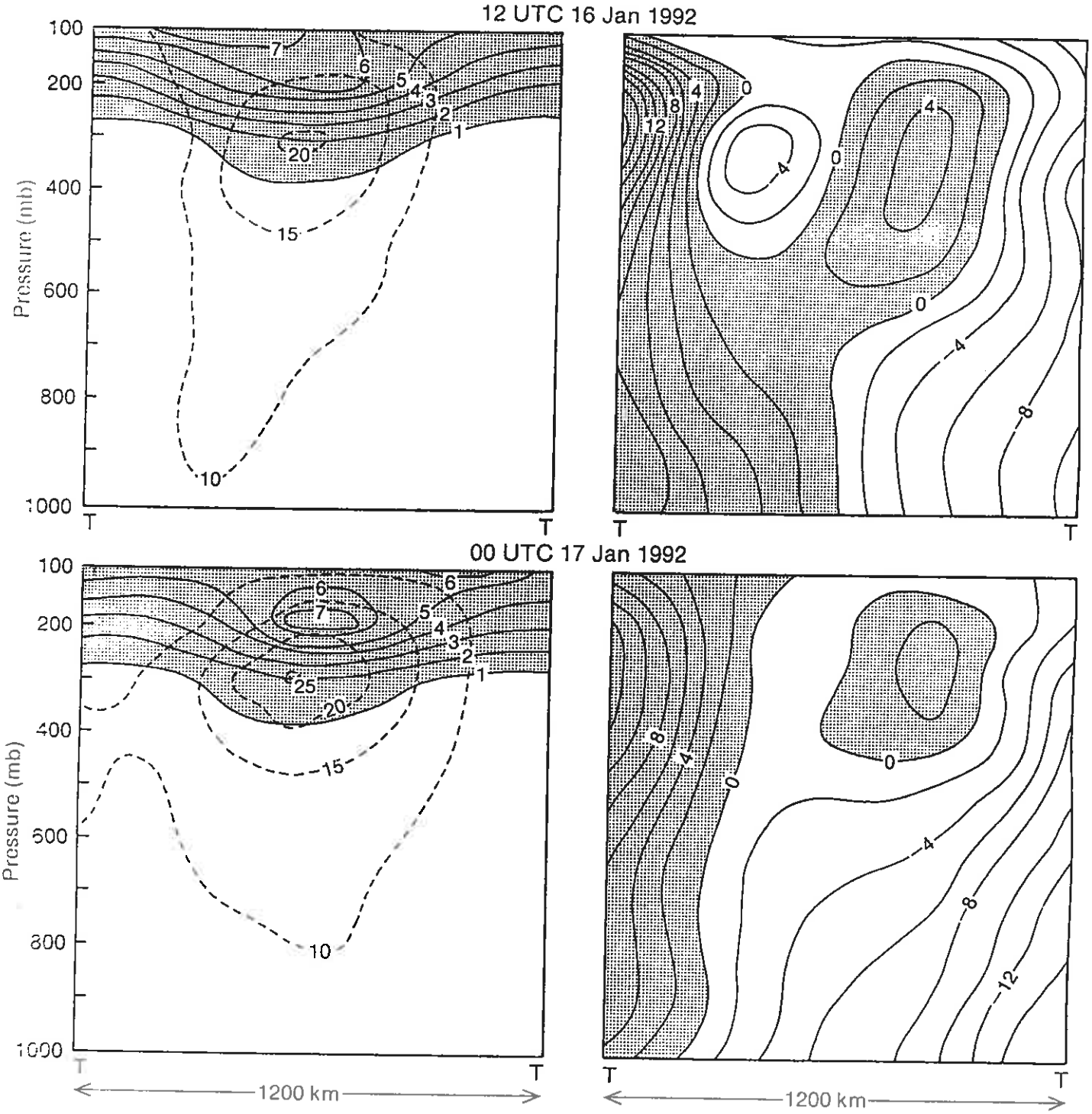

Fig 8(a) (second part)

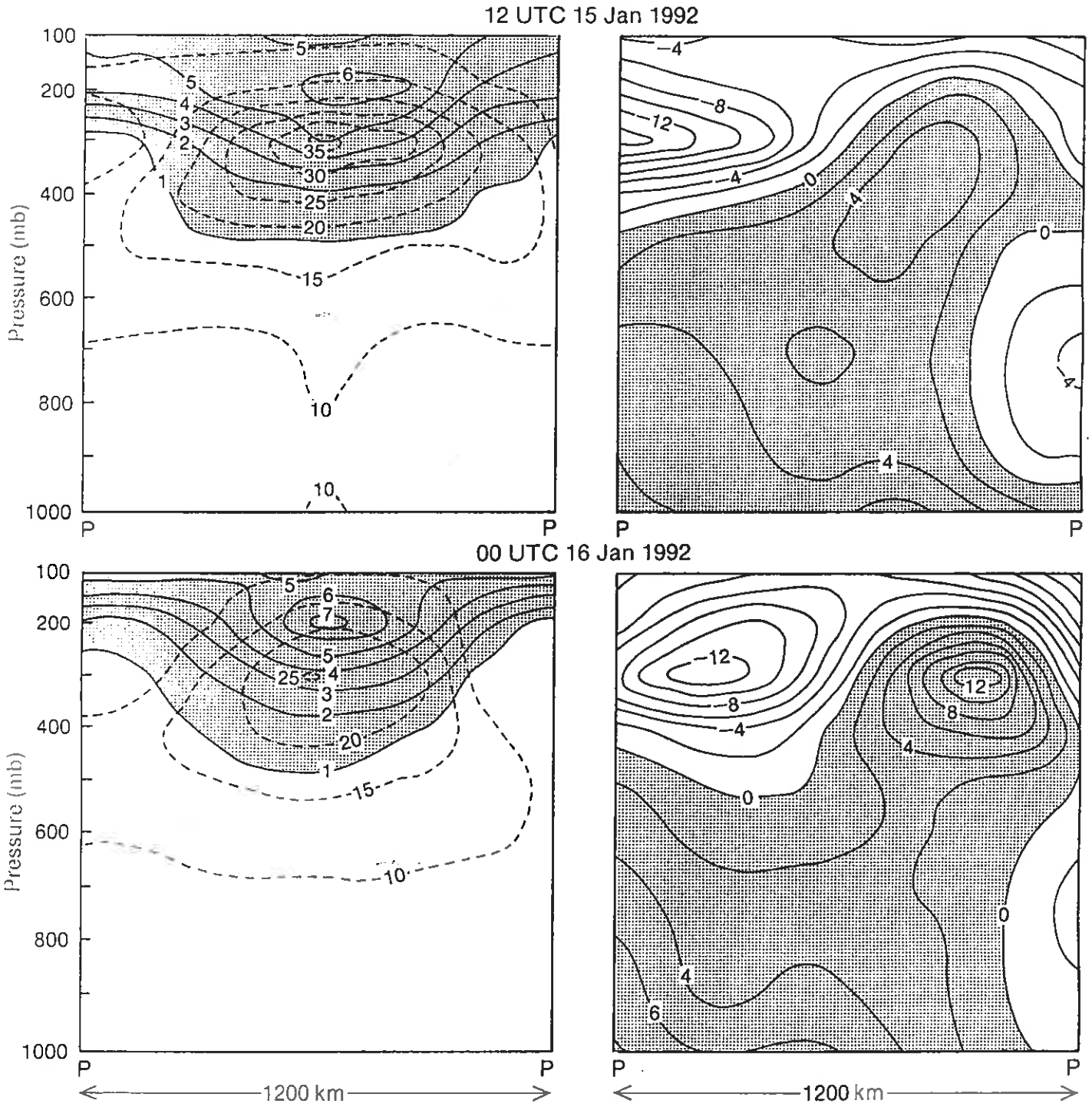

Fig 8(b) (first part)

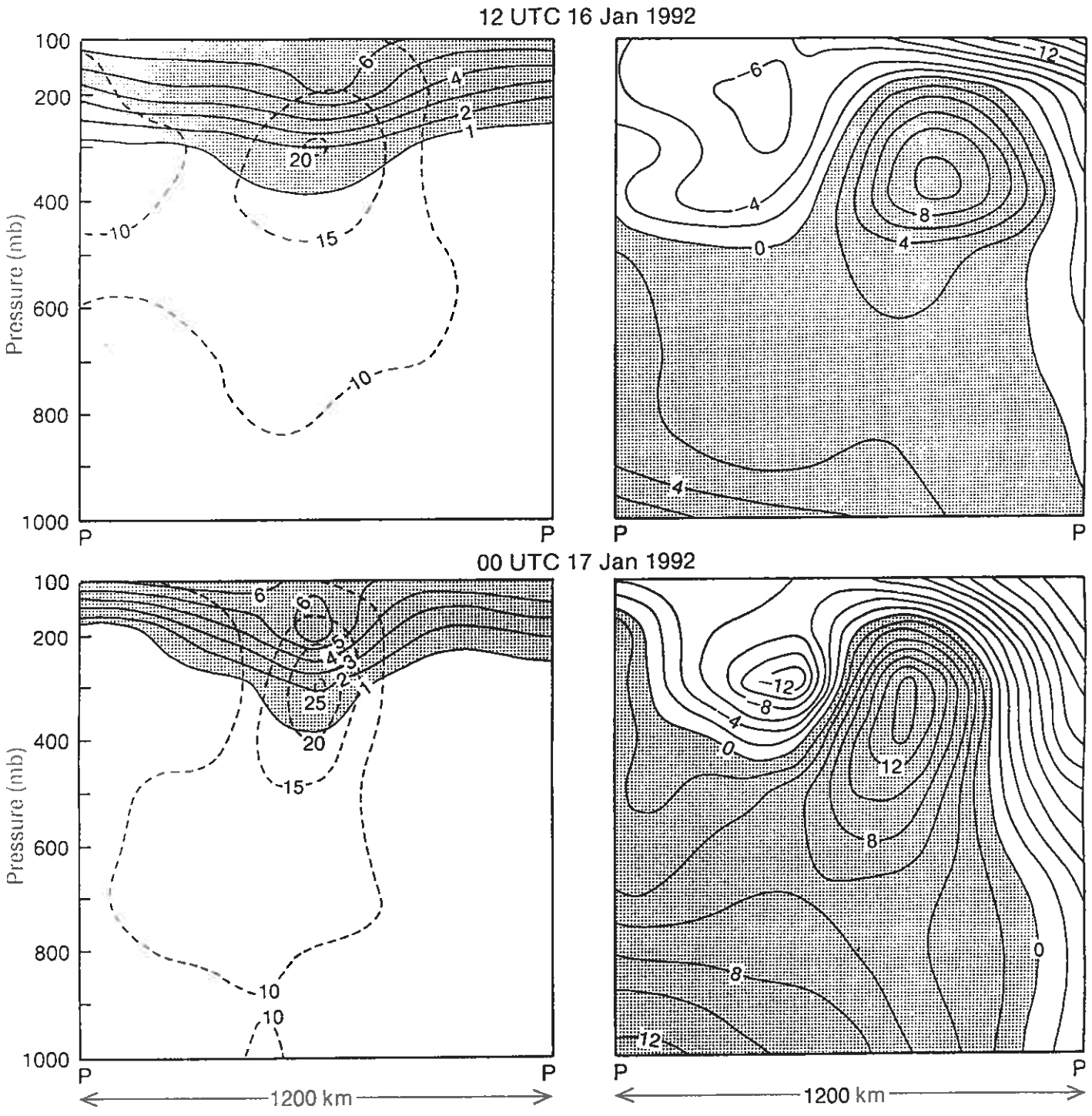

Fig 8(b) (second part)

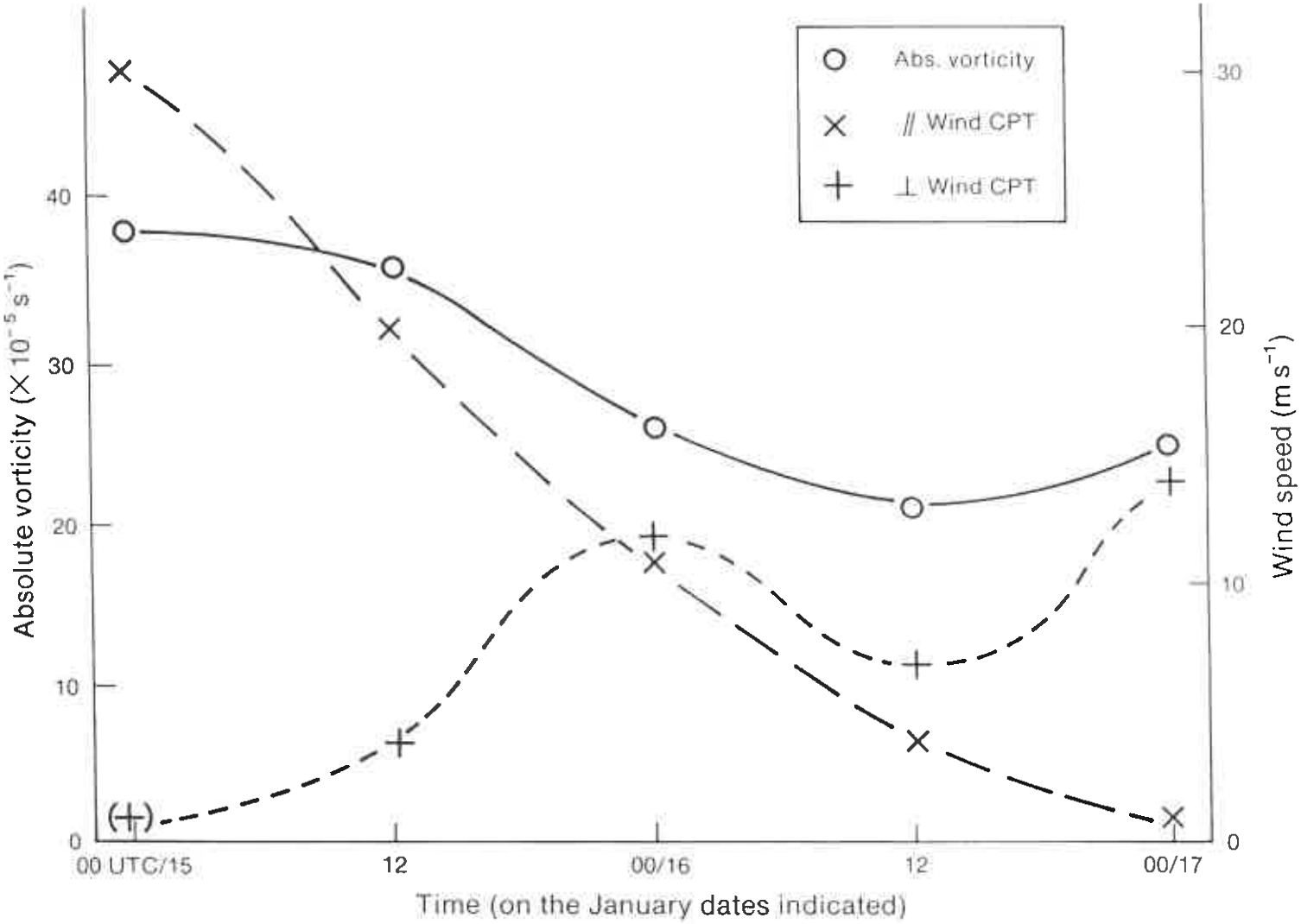
Abs. vorticity
// Wind CPT
⊥ Wind CPT
Absolute vorticity (× 10⁻⁵ s⁻¹)
Wind speed (m s⁻¹)
0
10
20
30
40
0
10
20
30
00 UTC/15
12
00/16
12
00/17
Time (on the January dates indicated)

Fig. 9

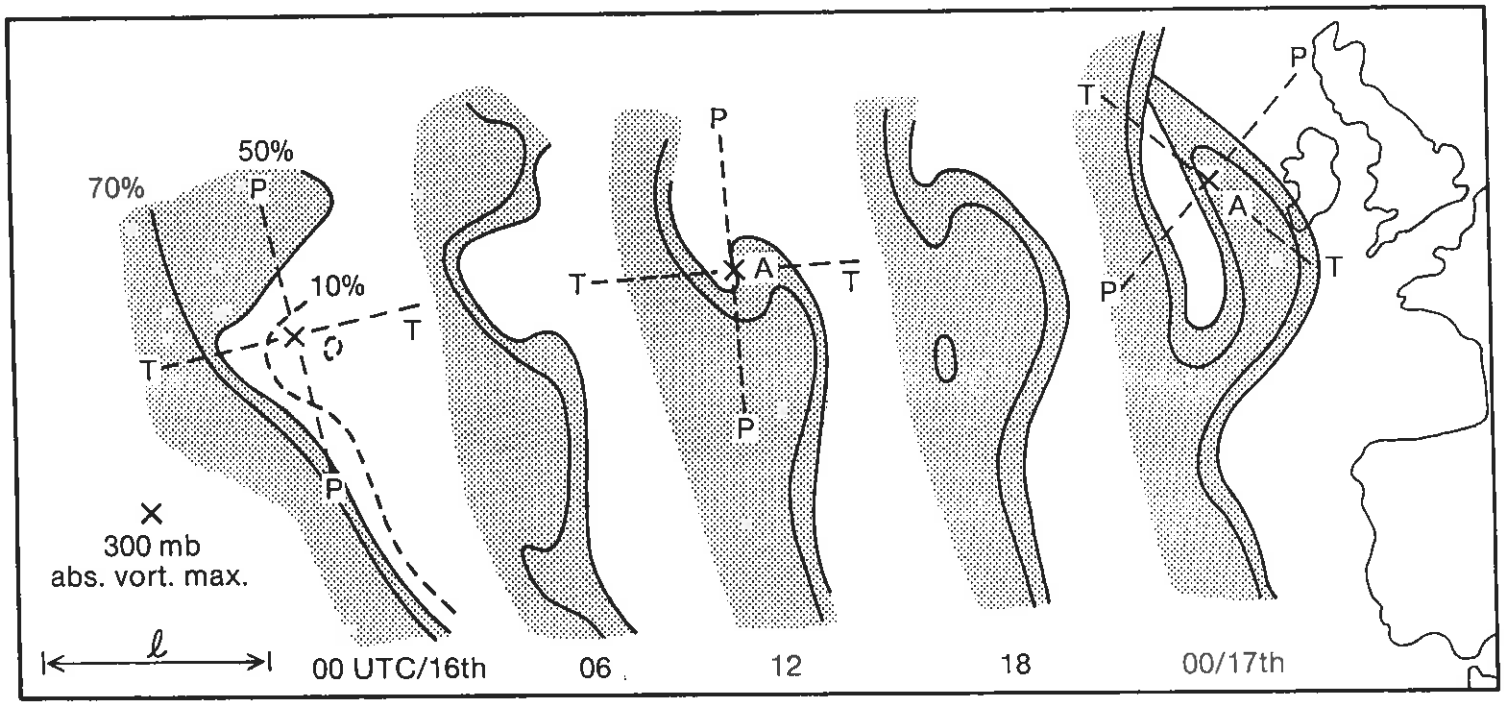
70%
50%
P
10%
T
T
P
300 mb
abs. vort. max.
ℓ
00 UTC/16th
T
P
A
T
P
06
12
18
P
T
A
T
P
00/17th

Fig 10

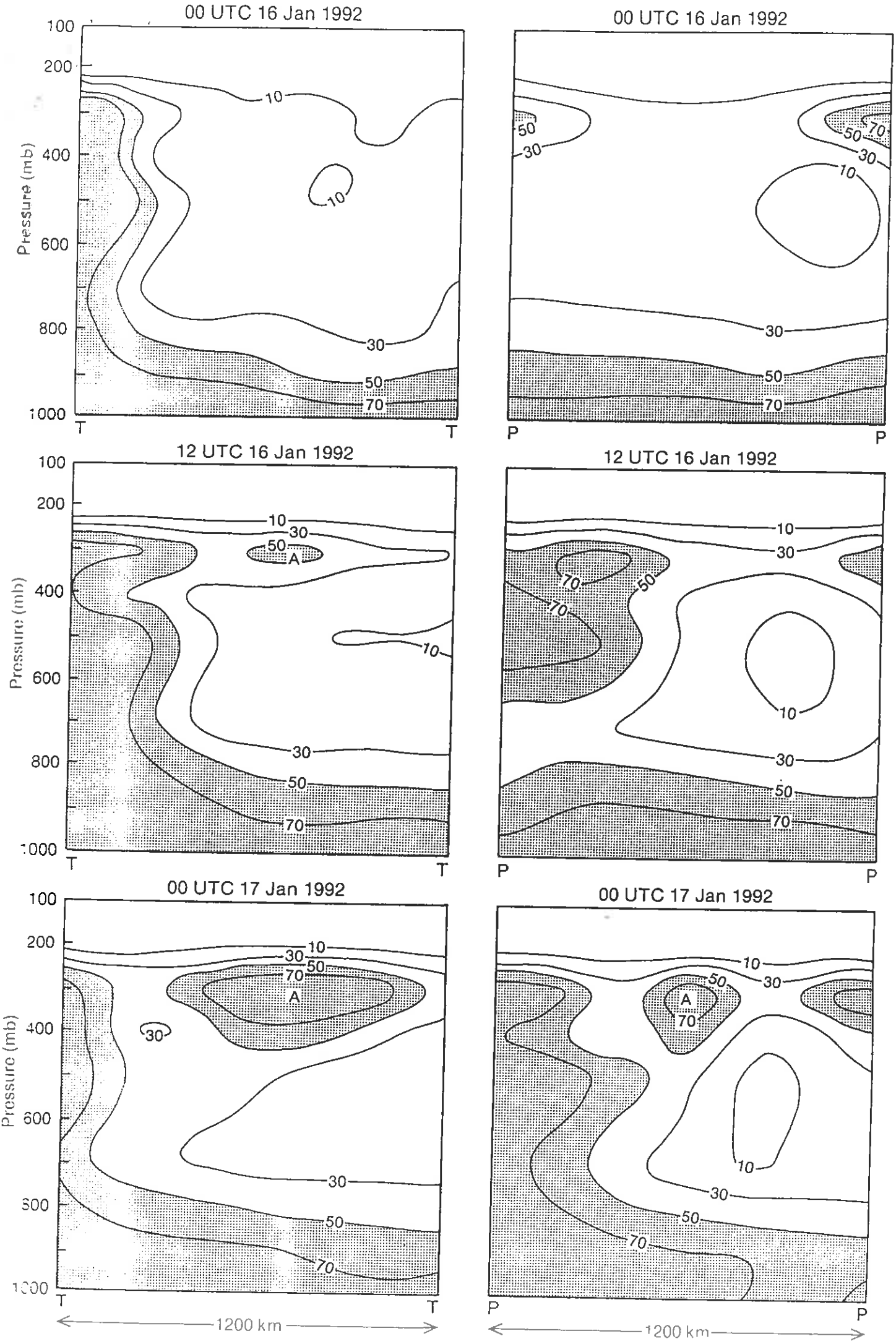
00 UTC 16 Jan 1992
00 UTC 16 Jan 1992
12 UTC 16 Jan 1992
12 UTC 16 Jan 1992
00 UTC 17 Jan 1992
00 UTC 17 Jan 1992
Pressure (mb)
100
200
400
600
800
1000
10
30
50
70
A
T
P
1200 km

Fig 11

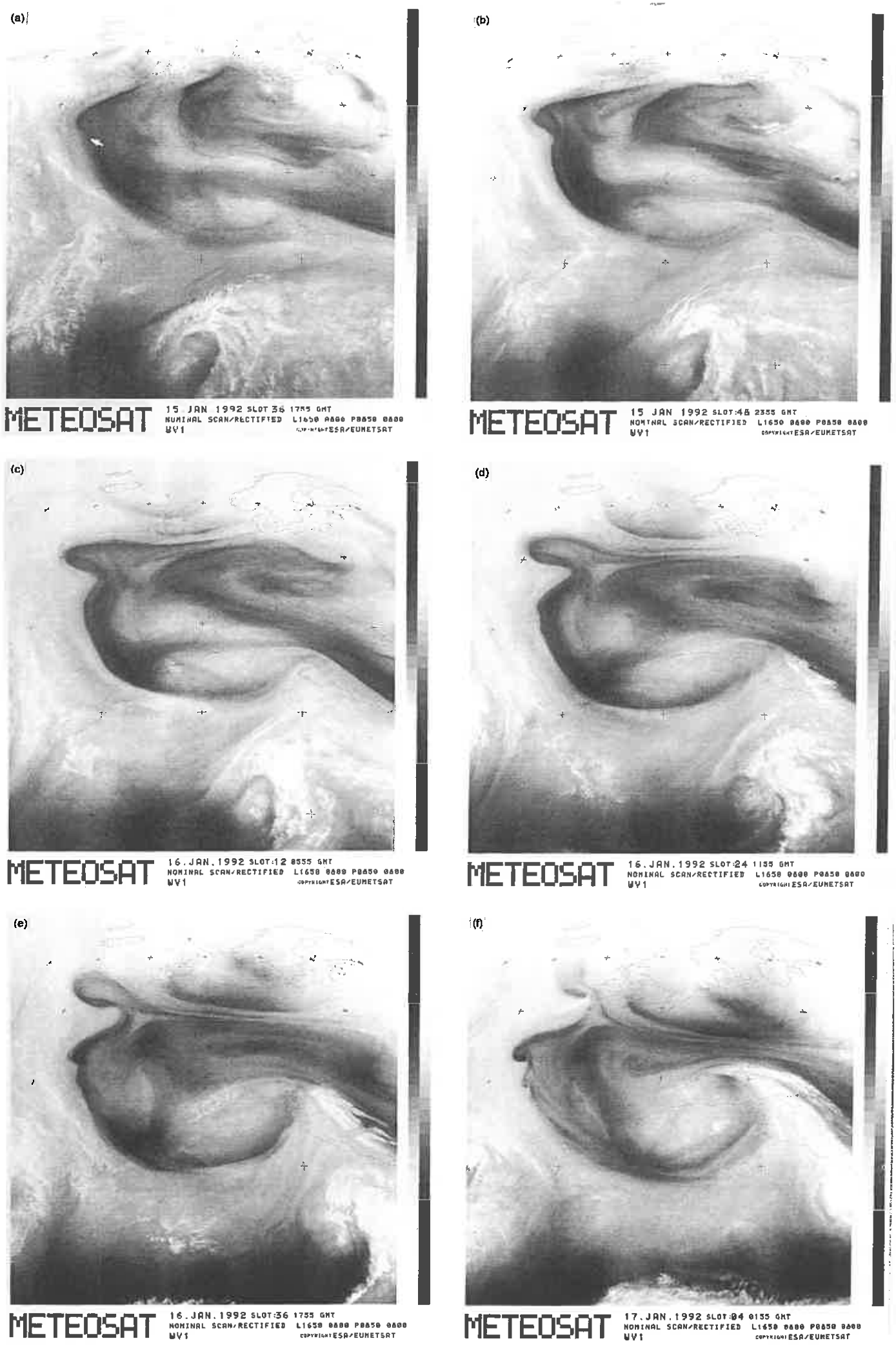
(a)
METEOSAT 15 JAN 1992 SLOT:36 1755 GMT
NOMINAL SCAN/RECTIFIED L1650 0800 P0850 0800
WV1
COPYRIGHT ESA/EUMETSAT
(b)
METEOSAT 15 JAN 1992 SLOT:48 2355 GMT
NOMINAL SCAN/RECTIFIED L1650 0800 P0850 0800
WV1
COPYRIGHT ESA/EUMETSAT
(c)
METEOSAT 16.JAN.1992 SLOT:12 0555 GMT
NOMINAL SCAN/RECTIFIED L1650 0800 P0850 0800
WV1
COPYRIGHT ESA/EUMETSAT
(d)
METEOSAT 16.JAN.1992 SLOT:24 1155 GMT
NOMINAL SCAN/RECTIFIED L1650 0800 P0850 0800
WV1
COPYRIGHT ESA/EUMETSAT
(e)
METEOSAT 16.JAN.1992 SLOT:36 1755 GMT
NOMINAL SCAN/RECTIFIED L1650 0800 P0850 0800
WV1
COPYRIGHT ESA/EUMETSAT
(f)
METEOSAT 17.JAN.1992 SLOT:04 0155 GMT
NOMINAL SCAN/RECTIFIED L1650 0800 P0850 0800
WV1
COPYRIGHT ESA/EUMETSAT

Fig 12

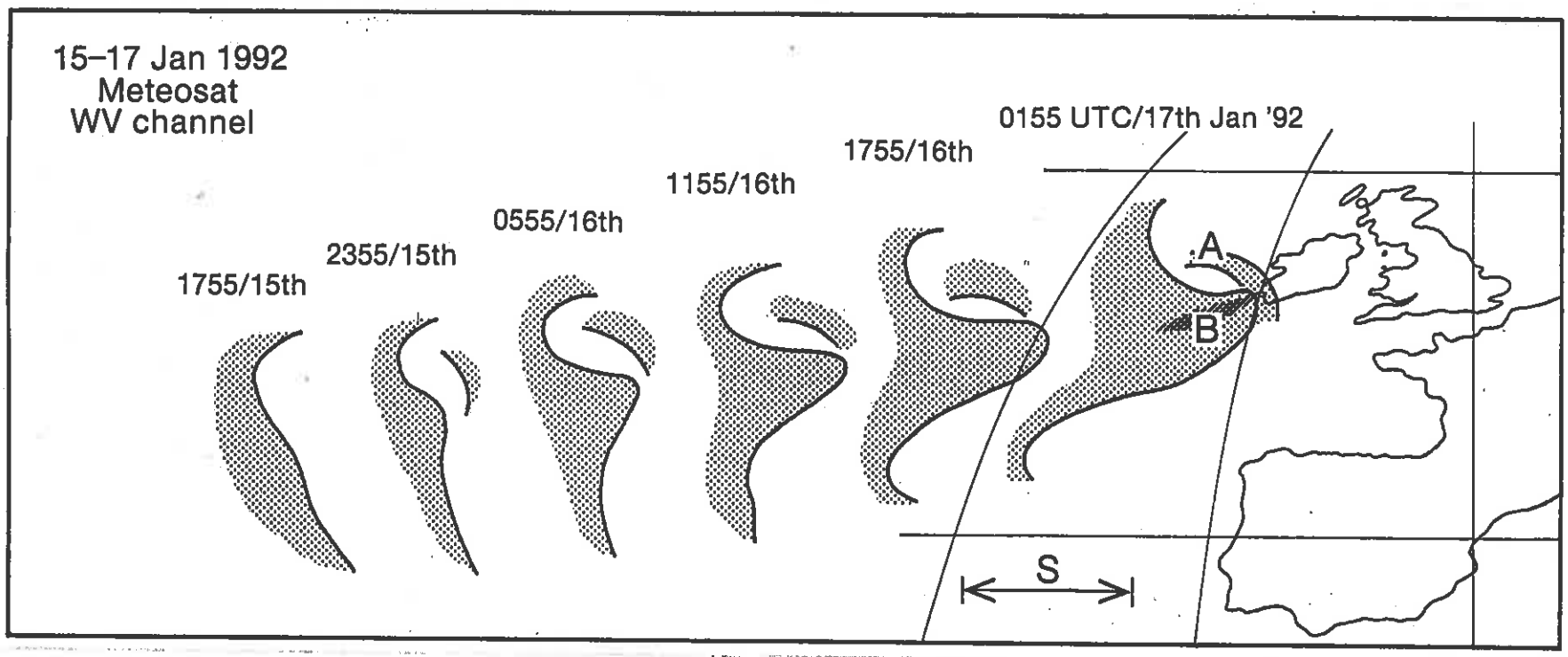
15–17 Jan 1992
Meteosat
WV channel
1755/15th
2355/15th
0555/16th
1155/16th
1755/16th
0155 UTC/17th Jan '92
A
B
S

Fig 13

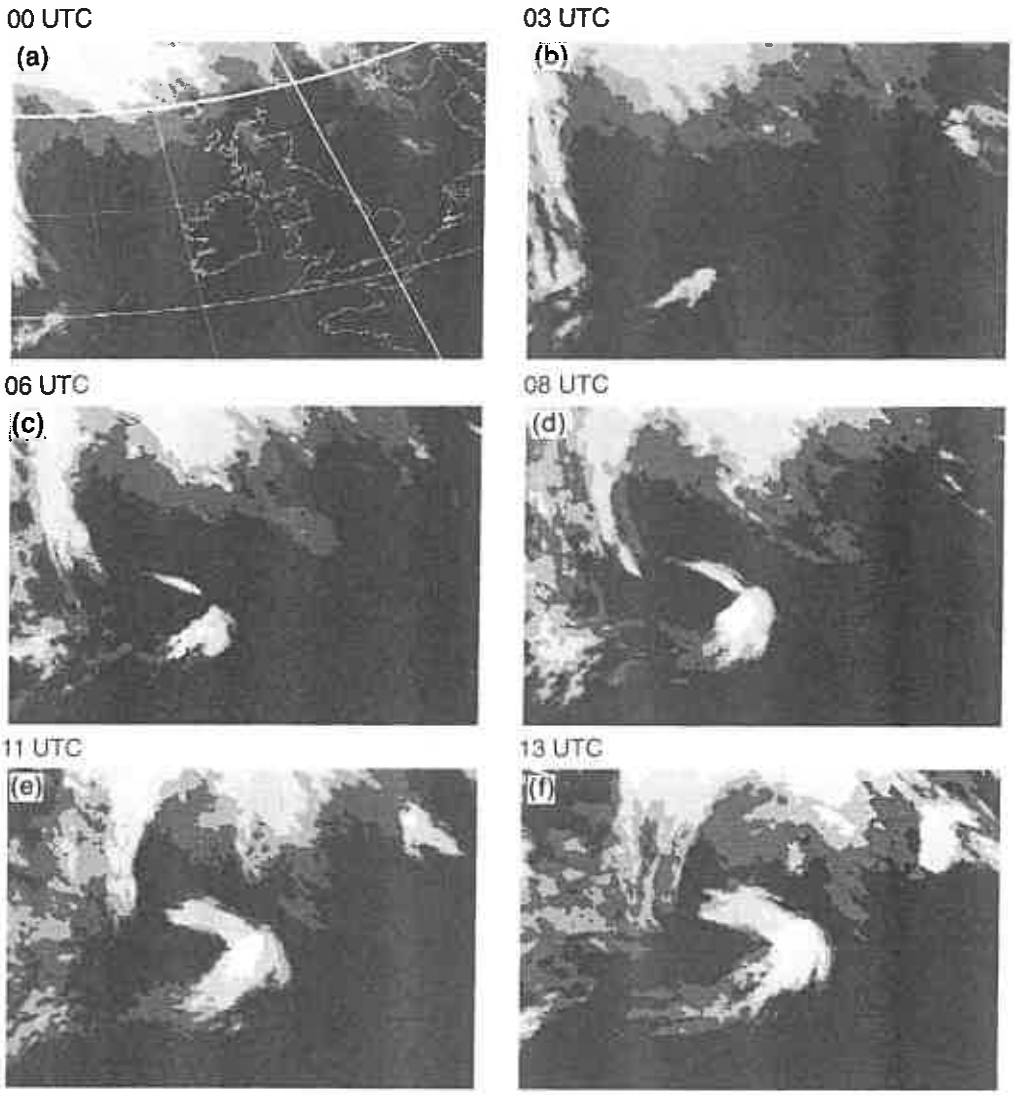

Figure 14

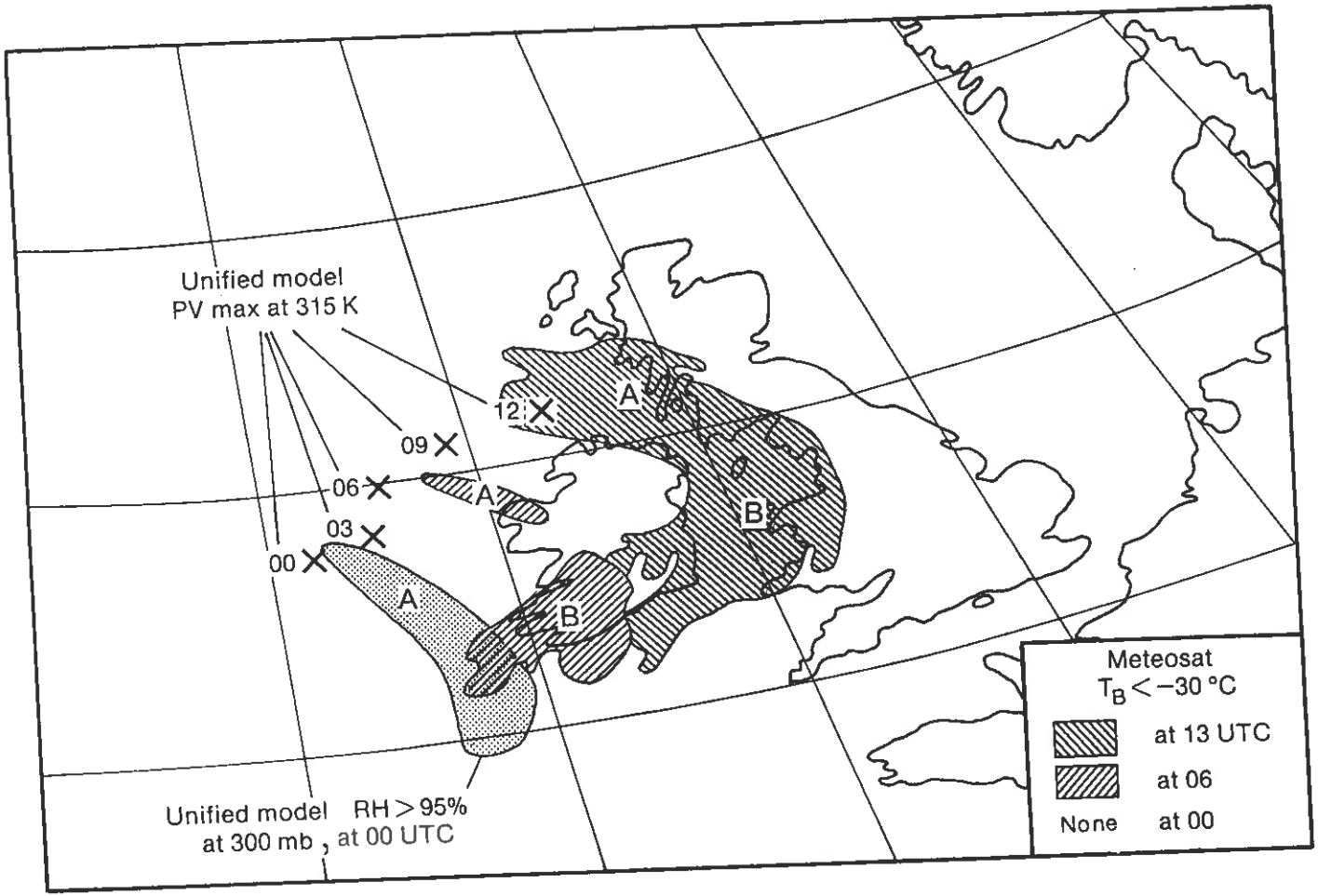
Unified model
PV max at 315 K
12
09
06
03
00
A
A
B
B
A
Unified model RH > 95%
at 300 mb , at 00 UTC
Meteosat
$T_B < -30$ °C
at 13 UTC
at 06
None
at 00

Fig 15

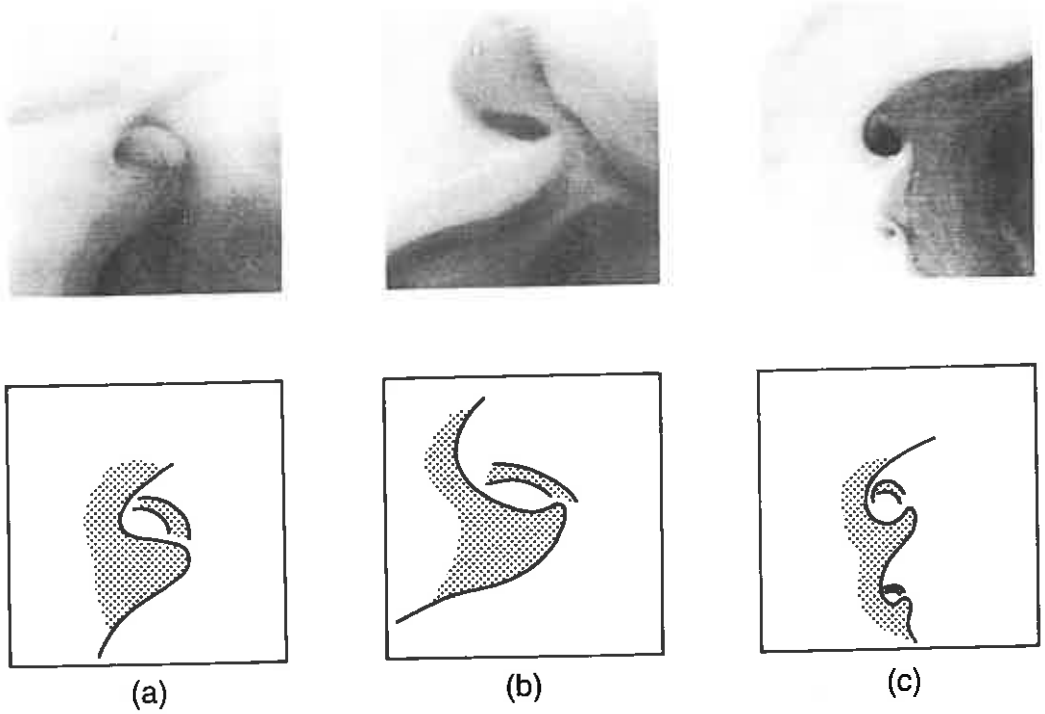

Fig 16

CURRENT JCMM INTERNAL REPORTS

This series of JCMM Internal Reports, initiated in 1993, contains unpublished reports and also versions of articles submitted for publication. The complete set of Internal Reports is available from the National Meteorological Library on loan, if required.

1. **Research Strategy and Programme.**
   K A Browning et al
   January 1993

2. **The GEWEX Cloud System Study (GCSS).**
   GEWEX Cloud System Science Team
   January 1993

3. **Evolution of a mesoscale upper tropospheric vorticity maximum and comma cloud from a cloud-free two-dimensional potential vorticity anomaly.**
   K A Browning
   January 1993

Met Office Joint Centre for Mesoscale Meteorology Department of Meteorology
University of Reading PO Box 243 Reading RG6 6BB United Kingdom
Tel: +44 (0)118 931 8425 Fax: +44 (0)118 931 8791
www.metoffice.com